



1 **Future water storage changes over the Mediterranean, Middle East, and North Africa in**
2 **response to global warming and stratospheric aerosol intervention**

3 **Abolfazl Rezaei^{1,2}, Khalil Karami³, Simone Tilmes⁴, John C. Moore⁵**

4 ¹ Department of Earth Sciences, Institute for Advanced Studies in Basic Sciences (IASBS), Zanjan
5 45137-66731, Iran. arezaei@iasbs.ac.ir; abolfazlrezaei64@gmail.com.

6 ² Center for Research in Climate Change and Global Warming (CRCC), Institute for Advanced Studies
7 in Basic Sciences (IASBS), Zanjan 45137-66731, Iran

8 ³ Institut für Meteorologie, Stephanstraße 3, 04103 Leipzig, Germany. khalil.karami@uni-leipzig.de

9 ⁴ National Center for Atmospheric Research, Boulder, CO, USA. tilmes@ucar.edu

10 ⁵ Arctic Centre, University of Lapland, Rovaniemi, 96101, Finland. john.moore.bnu@gmail.com

11

12 **Abstract**

13 Water storage plays a profound role in the lives of people across the Middle East and North Africa
14 (MENA) as it is the most water stressed region worldwide. The lands around the Caspian and
15 Mediterranean Seas are simulated to be very sensitive to future climate warming. Available water
16 capacity depends on hydroclimate variables such as temperature and precipitation that will depend
17 on socioeconomic pathways and changes in climate. This work explores changes in both the mean
18 and extreme terrestrial water storage (TWS) under an unmitigated greenhouse gas (GHG) scenario
19 (SSP5-8.5) and stratospheric aerosol intervention (SAI) designed to offset GHG-induced warming
20 above 1.5 °C and compares both with historical period simulations. Both mean and extreme TWS are
21 projected to significantly decrease under SSP5-8.5 over the domain, except for the Arabian Peninsula,
22 particularly in the wetter lands around the Caspian and Mediterranean Seas. Relative to global
23 warming, SAI partially ameliorates the decreased mean TWS in the wet regions while it has no
24 significant effect on the increased TWS in drier lands. In the entire domain studied, the mean TWS is
25 larger under SAI than pure greenhouse gas forcing, mainly due to the significant cooling, and in turn,
26 a substantial decrease of evapotranspiration under SAI relative to SSP5-8.5. Changes in extreme
27 water storage excursions under global warming are reduced by SAI. Extreme TWS under both future
28 climate scenarios are larger than throughout the historical period across Iran, Iraq, and the Arabian
29 Peninsula, but the response of the more continental eastern North Africa hyper-arid climate is
30 different from the neighboring dry lands.

31 **Keywords:** Mean and extreme water storage; SSP5-8.5; Stratospheric Aerosol Intervention; Global
32 warming; MENA region, Caspian and Mediterranean Seas

33



34 **500-character non-technical text**

35 Water storage (WS) plays a profound role in the lives of people in the Middle East and North Africa
36 and Mediterranean climate "hot spots". Simulated is WS changed by greenhouse gas (GHG) warming
37 with and without stratospheric aerosol intervention (SAI). WS significantly increases in the Arabian
38 Peninsula and decreases around Mediterranean under GHG. While SAI partially ameliorates the GHG
39 impacts, Projected WS increases in dry regions and decreases in wet areas relative to present climate.
40

41 **1. Introduction**

42 The Middle East and North Africa (MENA), with 6% of the world's population, are currently among
43 the most water-stressed regions worldwide (Fragaszy et al., 2020). The dry climate, intensifying
44 droughts, increasing population, and water over-extraction particularly across the Middle East
45 (World Bank, 2017), make it home to 12 of the 17 most water-stressed countries on the planet
46 (Hofste et al., 2019). Water availability is crucial for sanitation (Reiter et al., 2004), economic activity
47 (UNESCO, 2003), ecosystems (Shiklomanov and Rodda, 2003), and hydrological systems (Mooney et
48 al., 2005).

49

50 The MENA region has the largest expected economic losses from climate-related water scarcity,
51 robustly estimated at 6–14 % of Gross Domestic Product (GDP) by 2050 (World Bank, 2017). MENA's
52 terrestrial water storage (TWS) is being intensively extracted and may act as a flashpoint for conflict
53 (Famiglietti, 2014). TWS incorporates all water on the land surface (snow, ice, water stored in the
54 vegetation, river, and lake water) and in the subsurface (soil moisture and groundwater). Beyond
55 anthropogenic activities, natural climate variability such as drought frequency affects water storage
56 and agriculture, which then impacts food security (Fragaszy et al., 2020). The Middle East is
57 especially prone to severe and sustained droughts due to its location in the descending limb of the
58 Hadley circulation and associated dry and semiarid climate (Barlow et al., 2016). The 1998-2012 14-
59 year period was the worst drought in the past 900 years (Cook et al., 2016). Because the saturated
60 vapor pressure of air is largely controlled by temperature, any change in temperature, as well as
61 precipitation, substantially affects (Konapala et al., 2020; Ajjur and Al-Ghamdi, 2021; Hobeichi et al.,
62 2022) the water storage capacity available to supply the increasing water demand in the region (Lian,
63 2021). The MENA region, having both low precipitation and high evaporation, is very vulnerable to
64 climate change (Giorgi, 2006; IPCC, 2007; Lelieveld et al., 2012; Tabari and Willems, 2018; Zittis et
65 al., 2019). MENA water storage is therefore particularly sensitive to any perturbation of the water
66 cycle imposed by global warming.



67

68 Although MENA's adjacent densely populated region, the Mediterranean, has a better water storage
69 state, it is projected to substantially suffer from reduced water availability under future GHG climate
70 scenarios (Lionello et al., 2006). This is due to both projected significant decreases in rainfall
71 (Azzopardi et al., 2020) and large increases in demand for irrigation water by the end of the 21st
72 century (Fader et al. 2016).

73

74 If global mean surface temperature rises to exceed 1.5 °C above the preindustrial mean temperature,
75 severe global consequences, and societal problems can be expected (Masson-Delmotte, 2022). Solar
76 radiation modification (SRM), a form of intervention to cool the climate by reflecting sunlight, has
77 been proposed as a potential method of limiting global temperature rises and the associated impacts
78 of increased GHG emissions. SRM is likely the only way to keep or reduce surface temperatures to
79 1.5C given the reality of the GHG mitigation measures that have been agreed to date (MacMartin et
80 al., 2022). Simulations have shown a 2% decrease in total solar irradiance roughly offsets global
81 warming due to a doubling of CO₂ concentrations, and continuous injections of 10-18 Tg SO₂ would
82 lead to a cooling of about 1 °C after several years (WMO, 2022). This is consistent with observed
83 surface cooling after large volcanic eruptions, such as the 1991 Mt Pinatubo eruption which produced
84 cooling of about 0.3 °C over a 2-3 year period (e.g., IPCC, 2021).

85

86 GHG warming has already adversely affected water resources in the MENA region (Wang et al., 2018)
87 and is simulated to intensify water competition between states (Arnell, 1999) in the future. Although
88 global warming is expected to increase precipitation and soil moisture across MENA (Cook et al.,
89 2020), it will decrease runoff and groundwater recharge by larger amounts (Milly et al., 2005; Suppan
90 et al., 2008; Shaban 2008). Using GHG emission scenario A1B simulated by nine CMIP3-class climate
91 models, Droogers et al. (2012) projected that 22 % of the future annual water shortage, 199 km³ in
92 2050 in MENA, will be due to global warming. GHG-driven groundwater storage depletion in the
93 Middle East during the 21st century will far exceed that during the 20th century due to the increased
94 evapotranspiration (ET) and reduced volume of snowmelt (Wu et al., 2020).

95

96 The precipitation and water availability in the Mediterranean region, to the northwest of the MENA,
97 is also projected to be highly sensitive to global warming, having the largest differences in the water
98 availability between 1.5 and 2°C warming scenarios globally (Schleussner et al., 2016). Global
99 warming decreases Mediterranean groundwater recharge according to simulations under the IPCC



100 A2 and B2 scenarios simulated using ECHAM4 and HadCM3 models (Döll and Flörke, 2005). Runoff
101 is decreased by 10-30% according to 12 models such as CCSM3, and ECHAM5/MPI-OM (Milly et al.,
102 2005), and soil moisture z-scores by -1 to -4 in warm seasons according to simulations under SSP1-
103 2.6, SSP2-4.5, SSP3-7.0, and SSP5-8.5 (Cook et al., 2020). Water availability in turn is lowered by 8-
104 28% for a warming of 2 °C as simulated by 11 CMIP5-class models by Schleussner et al., (2016).
105 Likewise, Döll et al. (2018) found a strong drying in the Mediterranean region under global warming
106 since the largest precipitation decreases worldwide were simulated in this region under SSP1-2.6,
107 SSP2-4.5, SSP3-7.0, and SSP5-8.5 scenarios (Cook et al., 2020).

108

109 Many global climate models have simulated SRM in the form of stratospheric aerosol intervention
110 (SAI). Model studies include the Stratospheric Aerosol Geoengineering Large Ensemble Project
111 GLENS (e.g., Cheng et al., 2019; Simpson et al., 2019; Abiodun et al., 2021), the Geoengineering Model
112 Intercomparison Project (Kravitz et al., 2013; Tilmes et al., 2013), as well as others (e.g., Bala et al.,
113 2008; Jones et al., 2018; Muthyala et al., 2018). Compared with global warming, SAI decreases mean
114 global precipitation (Govindasamy and Caldeira, 2000; Bala et al., 2008; Robock et al., 2008; Cheng
115 et al., 2019; Simpson et al., 2019) as well as both the intensity and frequency of precipitation extremes
116 caused by GHG-induced climate change (Tilmes et al., 2013; Muthyala et al., 2018). Dagon and Schrag
117 (2016) is a rare article that focuses on the spatial variability of runoff and soil moisture responses to
118 SRM. Although solar geoengineering weakens the global hydrologic cycle (e.g., Bala et al., 2008;
119 Tilmes et al., 2013; Ricke et al., 2023), its regional impacts are method- and strategy-dependent
120 (Ricke et al., 2023) with potentially substantial changes in the regional precipitation patterns (Ricke
121 et al., 2010; Tilmes et al., 2013; Crook et al., 2015; Dagon and Schrag, 2016, Tilmes et al., 2020). While
122 differences in temperature fields vary relatively smoothly with radiative forcing, precipitation
123 patterns are far more variable being dependent on atmosphere/ocean/land surface coupling on a
124 wide range of spatial and temporal scales. Furthermore, SAI simulations rely on many model-specific
125 details and parameterizations that tend to produce larger across-model differences than simulations
126 using simpler forms of SRM (Visioni et al., 2021). While SAI may counteract the annual-mean water
127 availability changes over land forced by GHG, it is not easy to offset the regional consequences (Jones
128 et al., 2018), especially in the hydrological cycle.

129

130 Although the MENA region and the adjacent Mediterranean region are known to be a “hot spot” for
131 climatic change (Giorgi and Lionello, 2008; Bucchignani et al 2018), little has been done on potential
132 changes in TWS across MENA especially under SRM climates. This study fills that knowledge gap and



133 explores the changes that may occur in TWS under i) a high GHG emissions scenario, ii) the same GHG
134 scenario combined with SAI designed to globally neutralize the GHG radiative forcing, and iii)
135 compares both future climates with the historical conditions (1985-2014) across the Mediterranean,
136 Middle East, and northern Africa.

137

138 **2. Data and Methods**

139 **2.1. Study Area**

140 The study area is composed of MENA and southern Europe to its north including the Caspian
141 and Mediterranean Seas. MENA covers the large region from Morocco in the west to Iran in the east,
142 containing all the Maghreb and the Middle Eastern countries from the 15°N to 45°N latitude and from
143 20°W to 63°E longitude (Fig. 1). As well as a water-stressed region, MENA, is a worldwide hot spot
144 for exacerbated extreme temperatures, aridity conditions, and drought (Giorgi and Lionello, 2008;
145 Bucchignani et al., 2018). According to the Koppen Climate Classification System (Peel et al., 2007),
146 MENA broadly has a hot and arid climate except for the coastal regions and highlands. Most of
147 northern Africa (NA) has a desert climate and 90% is covered by the Sahara Desert. The 2 m air
148 temperature rises to 50°C in summertime while the annual mean precipitation is less than 25 mm
149 (Faour et al., 2016). The Arid Steppe climate predominates in Morocco, Algeria and Tunisia with cold
150 winters (Faour et al., 2016) except for the Atlas Mountains which are cooler and wetter (annual mean
151 precipitation of ~500mm).

152

153 Across the Middle East, the largest amount of precipitation falls in four main regions: the
154 coastal eastern Mediterranean Sea, the south coast of the Caspian Sea, the western sides of the Zagros
155 Mountains across Iran and Iraq, and the southern tip of the Arabian Peninsula. The Middle East also
156 contains several major deserts having little to no precipitation: the Lut and Kavir deserts in middle
157 and eastern Iran, the Arabian Desert, the Syrian Desert, and the Negev in southern Israel. Middle East
158 precipitation often originates from moisture coming from the west over the Mediterranean Sea
159 (Evans and Smith, 2006). The Red Sea and the Persian Gulf are also source regions for the heaviest
160 precipitations across the area.

161

162 The Mediterranean area is also projected to be highly sensitive to global warming
163 (Schleussner et al., 2016), particularly regarding water availability (Lionello et al., 2006). It has mild
164 wet winters and warm to hot, dry summers as well as a complicated morphology, owing to the many



165 steep orogenic structures, distinct basins and gulfs, along with islands and peninsulas of various sizes
166 (Lionello et al., 2006).

167

168 Based on its full range of climate types, we divided the study area into six sub-regions (R1 to
169 R6) to explore the changes in hydroclimate variables under both global warming and SAI scenarios
170 (Fig. 1). The regions R1 to R6 respectively refer to the lands around the Caspian Sea, eastern Middle
171 East (largely containing Iran and Iraq), Mediterranean area, Arabian Peninsula, eastern NA, and
172 western NA. The climatology of each region is summarized in Table 1. The lands around the Caspian
173 and Mediterranean Seas with a cooler climate, have the highest precipitation and real
174 evapotranspiration (ET, the quantity of water actually removed from a surface by evaporation and
175 transpiration) while eastern NA with hyper-arid climate has the lowest precipitation, real ET, soil
176 moisture, and TWS. The lands around the Caspian Sea have the highest soil moisture and TWS.

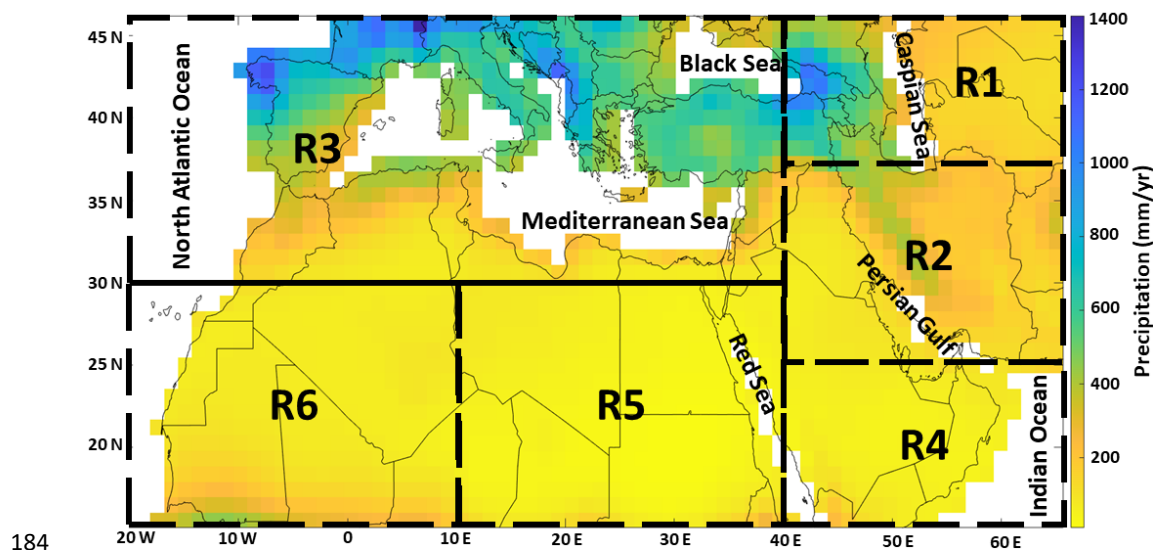
177

178 **Table 1.** The medians of precipitation, temperature, real evapotranspiration (ET), soil moisture,
179 terrestrial water storage (TWS), and potential ET over each region (R1 to R6, see Fig. 1) during the
180 historical period according to the model outputs. The results for global warming and SAI are further
181 shown in Table S1.

Region	R1	R2	R3	R4	R5	R6
Precipitation (mm/yr)	321	182	479	78	48	112
Temperature (°C)	14.2	20.5	17.2	27.0	23.7	25.3
Real ET (mm/yr)	419	187	388	72	50	112
Soil moisture (Kg/m ²)	1846	1771	1572	1353	1155	1287
TWS (Kg/m ²)	2091	1776	1623	1348	1167	1313
Potential ET (mm/yr)	74	123	74	210	143	185

182

183



184
 185 **Figure 1.** The MENA’s annual precipitation map during the historical period. Regions R1 to R6
 186 largely refer to the lands around the Caspian Sea, the eastern Middle East (largely containing Iran
 187 and Iraq), the Mediterranean area, Arabian Peninsula, eastern North Africa (NA), and western NA,
 188 respectively.
 189

190 **2.2. Model simulations and scenarios**

191 We examined the data from the NCAR Community Earth System Model version 2- Whole Atmosphere
 192 Community Climate Model Version 6 (CESM2(WACCM6)) that simulated the Coupled Model
 193 Intercomparison Project phase 6 (CMIP6; Eyring et al., 2016) scenarios. The SAI simulation we use
 194 (SSP5-8.5-SAI) is designed to employ SAI together with the high GHG emissions scenario, SSP5-8.5
 195 with the target of limiting the mean global temperatures to 1.5°C above the pre-industrial (1850–
 196 1900) conditions (Tilmes et al., 2020). Under SSP5-8.5 forcing, Tilmes et al. (2020) projected this
 197 threshold is exceeded around the year 2020 in CESM2(WACCM6). The atmospheric component of
 198 CESM2(WACCM6) has a resolution of 1.25° in longitude and 0.9° in latitude. The experiment injects
 199 SO₂ at 180° longitude at four predefined latitudes (30°N, 30°S, 15°N, and 15°S) at around 25 km in
 200 15°N/S and around 22 km at 30°N/S as suggested by Tilmes et al. (2018), using a feedback control
 201 algorithm to maintain not just the global mean temperature, but the interhemispheric and equator-
 202 to-pole temperature gradients (Tilmes et al., 2020). For SSP5-8.5-SAI, the largest aerosol volumes
 203 were injected at 15°S, modest mass at 15°N and 30°S, and a small amount at 30°N. We used the
 204 monthly TWS, precipitation, temperature, water evaporation from soil and canopy, transpiration,
 205 and soil moisture data from all five ensemble members (r1 to r5) of the SSP5-8.5 scenario and the
 206 three available ensemble members (1-3) of SSP5-8.5-SAI. The results for variables other than TWS



207 are shown in the Supplementary Information. For the historical period, we also used all three
208 available realizations (r1 to r3) from CESM2(WACCM6). For the anomaly analysis relative to
209 historical conditions and, in turn, the multiple linear regression models we used the first three
210 ensembles of SSP5-8.5, consistent with the three available historical members. We compare the GHG
211 and SAI scenarios over 2071-2100 with the 1985-2014 historical period.

212

213 2.3. Return periods

214 We are interested in climate extremes, not only changes in means. Therefore, we examine how the
215 frequency of events of some particular levels are likely to change under different scenarios. We use
216 the generalized extreme value (GEV) distribution function to estimate the probability distribution
217 function of the TWS extremes. A return period is an estimated average time between events such as
218 floods or river discharge flows. It is calculated by generating the 95% normal-approximate
219 confidence intervals in accordance with the mean and variance of the variable (here TWS).

220 The GEV distribution function is defined as (Gilleland, 2020):

$$221 \quad G(z) = \exp \left[- \left\{ 1 + \xi \left(\frac{z - \mu}{\sigma} \right) \right\}_+^{-1/\xi} \right] \quad (1)$$

222 where $\{\cdot\}_+$ denote that the value inside the bracket is set to zero when <0 . The GEV distribution is
223 parameterized using ξ , μ , and σ which are the shape, location, and scale parameters, respectively
224 and analogous to the skewness, mean and standard deviation. We assume that the GEV is the valid
225 distribution function for variables z_1, \dots, z_n representing the annual maximum return TWS levels,
226 where the quantiles of the distribution function give the return levels, z_p . The return levels are the
227 solutions to $G(z_p) = 1 - p$, which yields (Gilleland, 2020):

$$228 \quad z_p = \begin{cases} \mu - \frac{\sigma}{\xi} [1 - \{-\ln(1-p)\}^{-\xi}] & \text{for } \xi \neq 0 \\ \mu - \sigma \ln\{-\ln(1-p)\} & \text{for } \xi = 0 \end{cases} \quad (2)$$

229 p is probability corresponding to z_p . The return period is obtained as:

$$230 \quad \text{return period}(i) = 1 / (1 - \text{cdf}(i)) \quad (3)$$

231 where cdf is the cumulative distribution function. We also calculated the 95% asymptotic lower and upper
232 confidence intervals based on the Kolmogorov-Smirnov statistic (Doksum and Sievers, 1976). We used the
233 concatenated TWS anomaly data for the historical period, high GHG emissions, and SAI scenarios to
234 analyze the return periods.



235 **2.4. Multiple linear regression (MLR) model**

236 We want to analyze how the primary driving climate fields (surface air temperature, precipitation,
237 and evapotranspiration) for TWS vary spatially and among the different scenarios (Zhang et al.,
238 2022). We use a simple multiple linear regression (MLR) model with TWS as the dependent variable
239 (Y) for each ensemble member in each region. The following procedures were conducted:

240 i) We considered a linear regression model with potential independent variables (X): temperature,
241 precipitation, and real ET. We excluded soil moisture in X since its variability is highly correlated with
242 TWS changes (Fig. S2 in the Supplementary Information), so not an independent variable. Similarly,
243 potential ET (that is the amount of water that would be removed from a surface if a sufficient water
244 source were available) was excluded from the model due to its high spatial and temporal correlation
245 with temperature.

246 ii) Identifying the outliers using the Bonferroni p -values (i.e., Bonferroni correlation) and then
247 removing them. Bonferroni correlation is a modification for p -values when several dependent or
248 independent statistical tests are being accomplished concurrently on a single data set. A Bonferroni
249 correction divides the critical p -value by the number of comparisons being made (Bland and Altman,
250 1995).

251 iii) Fitting the final model after removing the outliers. In all regions and scenarios, the MLR models
252 are statistically significant at the 95% level. The variance explained (R^2) varies from around 0.3 in
253 the dry southern MENA to 0.8 in the wetter lands around the Caspian and Mediterranean Seas.

254 iv) Assessing the relative “importance” of the variables for TWS in the final model using the
255 Lindeman, Merenda, and Gold (LMG) method (Lindeman et al., 1980), where the fractional variance
256 accounted for is determined as the independent variable-order average over average contributions
257 in models of different sizes. LMG has been recommended by Johnson and LeBreton (2004)
258 and Grömping (2007) since it uses both direct effects and impacts adjusted for other regressors in
259 the model. Here we use all three ensemble members separately to estimate the robustness of the
260 importance estimates.

261

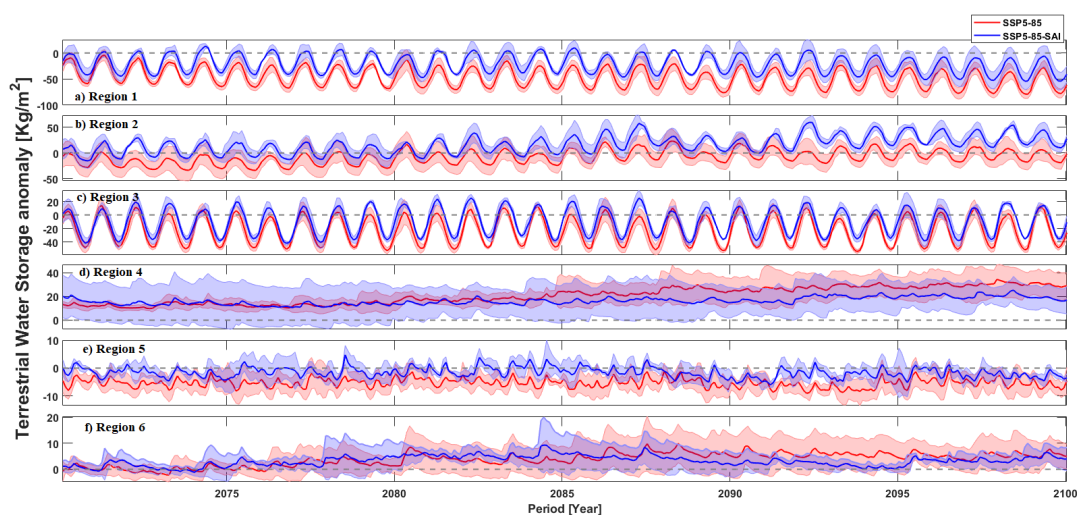
262 **3. Results:**

263 **3.1. Mean terrestrial water storage (TWS) changes due to GHG and SAI**

264 In this section, we present the projected changes in TWS across MENA and the lands around the
265 Caspian and Mediterranean Seas. We discuss trends in the TWS anomalies relative to TWS averaged
266 over the historical period (1985-2014) in response to both GHG (SSP5-8.5) forcing and to GHG+SAI.
267 The positive and negative anomalies in Fig. 2 refer to increasing and decreasing TWS, respectively.



268 The trend decreases in the northern parts (R1 and R3) and eastern NA (R5) with a hyper-arid climate
 269 but rises in the Arabian Peninsula (R4) and western NA (R6) under both GHG and SAI scenarios,
 270 particularly over the latter part of the 21st century. In all regions, the SAI climate TWS is higher than
 271 SSP5-8.5 or at least lies in the across-range of SSP5-8.5 towards the end of the century, especially in
 272 R2 and R5 (Fig. 2). For R2, the difference between SAI climate TWS is greater than in the rest of the
 273 domain, particularly over the latter part of the 21st century. The TWS change is smaller in the hyper-
 274 arid eastern NA (R5) than the other regions under both climate scenarios.

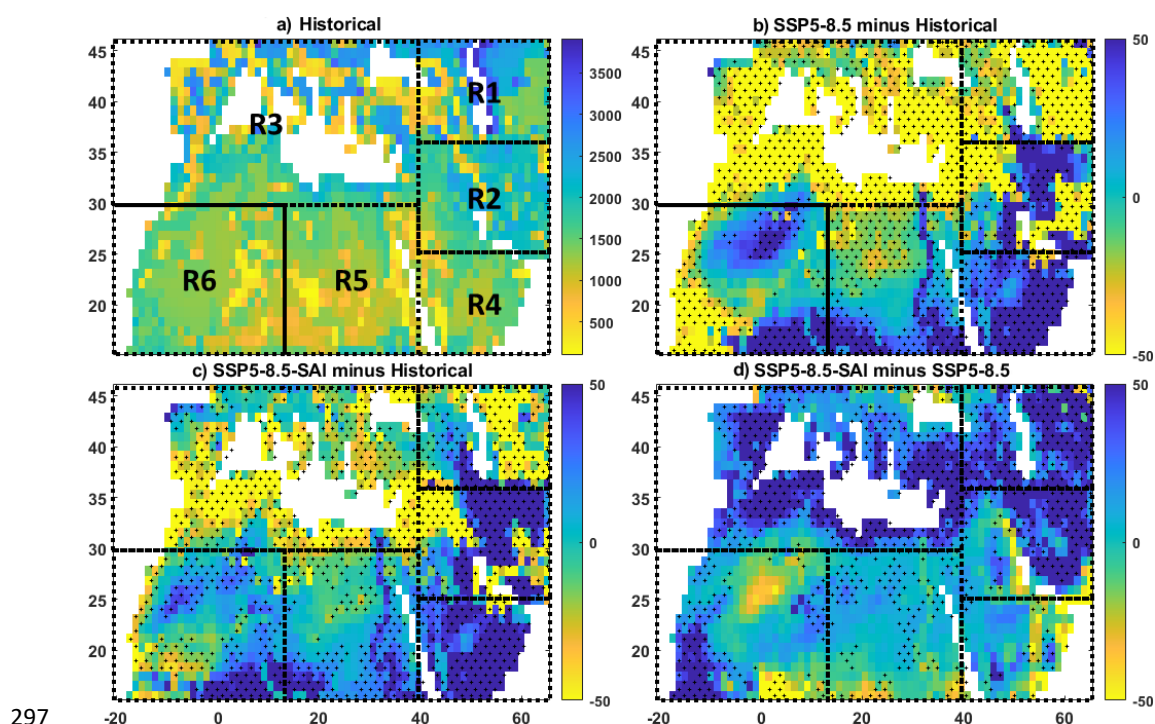


275
 276 **Figure 2.** The TWS anomaly relative to the TWS averaged over the historical period across MENA
 277 and the lands around the Caspian and Mediterranean Seas under global warming without (SSP5-
 278 8.5) and with SAI (SSP5-8.5-SAI). Figures a-f respectively are for regions R1 to R6. Shading in each
 279 curve shows the across-ensemble range. The dashed line crossing the y-axis at zero in each subplot
 280 is the ensemble mean of TWS over the historical period (1985-2014).

281
 282 Fig. 3 depicts the TWS differences between the historical (1985-2014) and the future climate
 283 scenarios over the 2071-2100 period. Consistent with the above findings, Figs. 3b and S1a-c show
 284 that the TWS response to GHG forcing in the wet regions around the Caspian and Mediterranean Seas
 285 is simulated as declining, while across the (semi)arid MENA region, particularly in central Iran, the
 286 Arabian Peninsula, and the southern portions of NA, there is a positive trend. Under global warming,
 287 the largest decrease in TWS occurs around the Caspian (particularly in the east) and the
 288 Mediterranean (except for its north) while its most robust increase happens in the southern margins
 289 of NA and the eastern parts of the Arabian Peninsula. SAI (Figs. 3c and S1d, e, and f) partially
 290 counteracts the changes imposed by the increased GHG emission, particularly in the wetter lands



291 around the Caspian and Mediterranean Seas which are simulated as experiencing TWS decrease
 292 under global warming. Mean TWS due to GHG forcing (Fig. 3b) is only partially reversed by SAI (Fig.
 293 3d), and the water storage shortfall is not fully canceled out by the intervention (Fig., 3c and d).
 294 However, simulated TWS in Iran and the southern half of MENA has greater water storage under SAI
 295 relative to the historical period (Fig. 3c).
 296



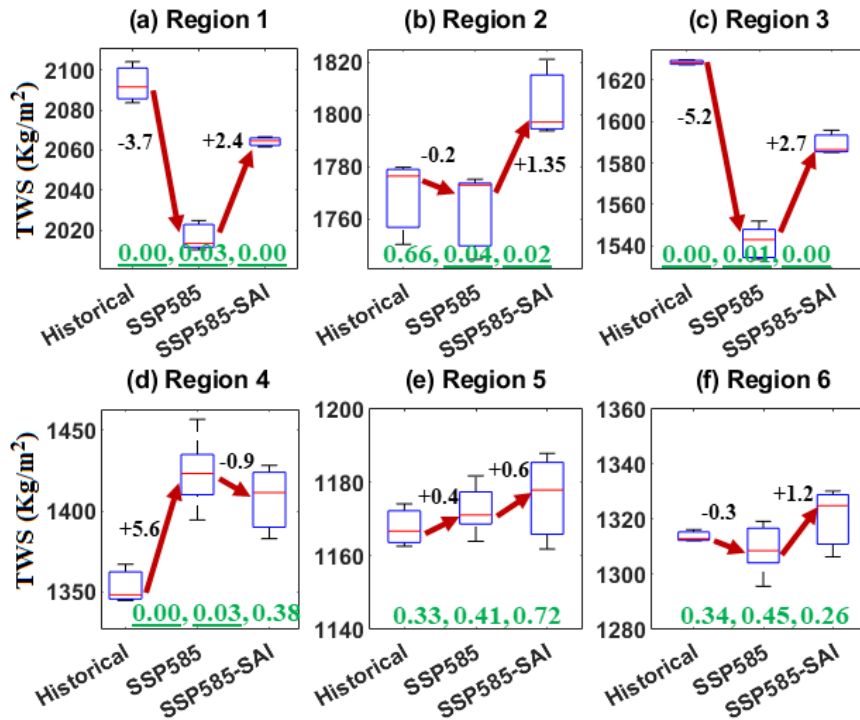
297
 298 **Figure 3.** Ensemble mean maps of TWS across the studied domain in the historical climate (a) over
 299 1985-2014 and their projected future changes in the 2071–2100 period under the SSP5-85 GHG
 300 scenario (SSP5-8.5 minus historical (b) and GHG+SAI minus historical (c)). The extent to which the
 301 SAI impacts the TWS changes imposed by global warming is further shown (SAI minus SSP5-8.5
 302 (d)). Hatched areas show where all ensemble members agree on the sign of the changes.

303

304 In Fig. 4 we compare how simulated TWS statistical distributions vary between scenarios for each
 305 region. Mean TWS significantly ($p < 0.05$) decreases in the wetter lands around the Caspian (R1) and
 306 Mediterranean (R3) Seas to the north ($35\text{--}58 \text{ Kg/m}^2$ on area average) while it significantly increases
 307 in the dry region of Arabian Peninsula (75 Kg/m^2) in response to GHG warming. SAI, on the whole,
 308 partially reverses the projected changes in TWS from increasing GHG concentrations toward its
 309 historical values. Interestingly, SAI overcompensates the TWS changes imposed by the high GHG



310 forcing in Iran and Iraq (R2) where this region shows no significant change under GHG emissions
 311 (Figs. 4b).
 312



313 **Figure 4.** Box and whiskers plot of the changes in the Terrestrial Water Storage (TWS) in regions 1
 314 to 6 over 2071-2100 under SSP5-8.5 and SSP5-8.5-SAI relative to historical conditions (1985-
 315 2014). The titles of each subplot refer to the regions. The median for each experiment is denoted by
 316 the red line, the upper (75th) and lower (25th) quartiles by the top and bottom of the box, and
 317 ensemble limits by the whisker extents. The positive/negative values in black are the change
 318 percent under SSP5-8.5 and SSP5-8.5-SAI relative to the median of the historical period data. The
 319 three values in green refer to *p*-values obtained from *t*-test analysis in which the underlined *p*-
 320 values are statistically significant.
 321
 322

323 3.2 Changes in extreme TWS

324 We compared changes in the expected return frequency of comparatively rare events to those during
 325 the historical period. Changes in mean conditions discussed so far are clear, but the changes in
 326 extremes display even larger separations between those expected under pure GHG forcing and the
 327 GHG+SAI scenarios. An increase in the return level or decrease in the return period of TWS means
 328 that the rare levels of high water availability increase, while a decrease in return level for a given
 329 period means that rich water availability events become rarer. Fig. 5 shows the return levels versus
 330 return period curves with the 95% lower and upper bands. If one curve, including its bands, does not

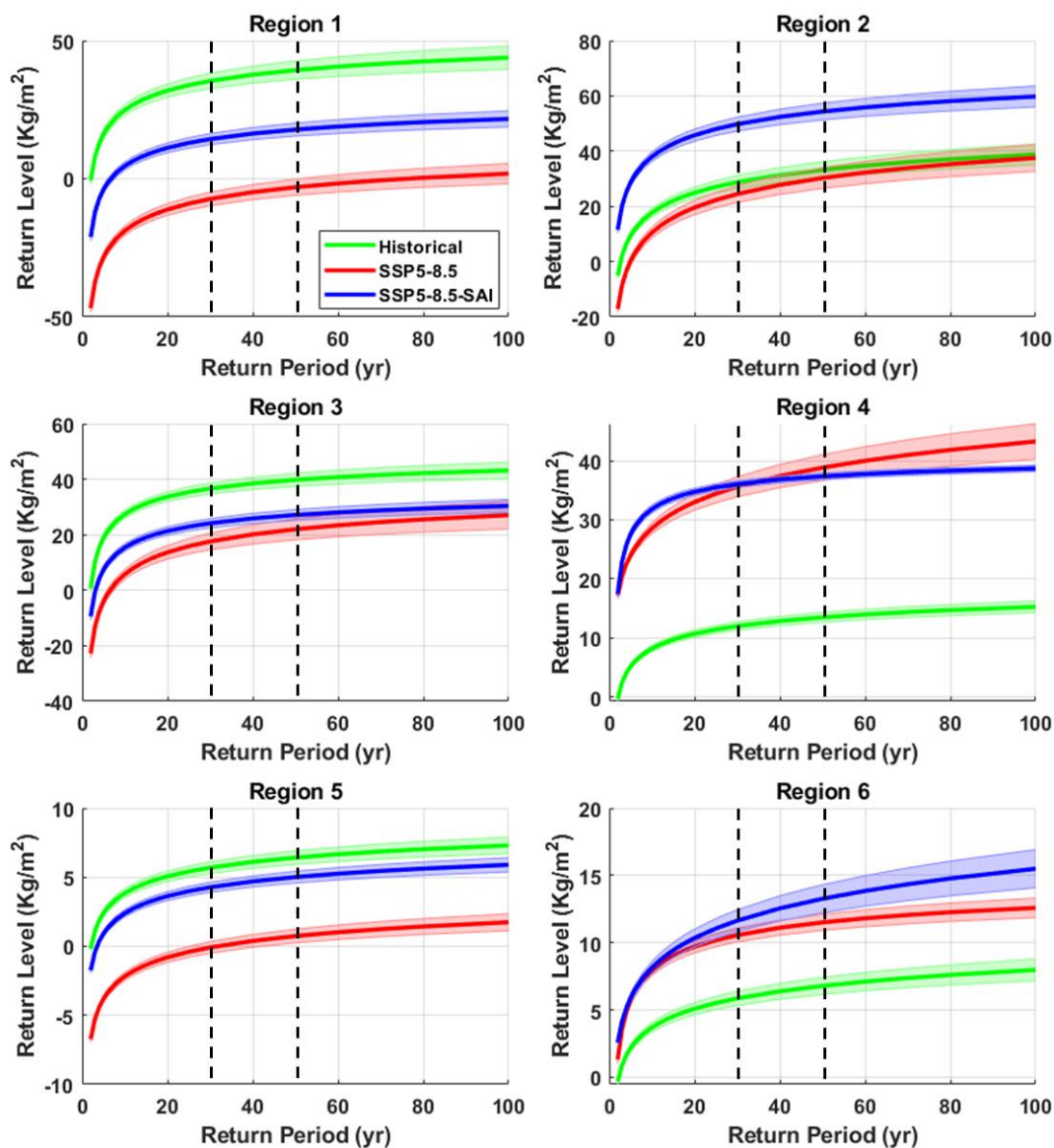


331 overlap its adjacent curve, we can say that the change at that return period is significant. The
332 expected return levels versus return period curves (Fig. 5) decrease in response to both GHG
333 warming and GHG+SAI in the Caspian and Mediterranean Seas area (R1 and R3) as well as in the
334 eastern NA (R5) as a more continental dry land but increase in the Arabian Peninsula (R4) and
335 western NA (R6). In Iran and Iraq (R2), SAI leads to a significant increase in expected TWS level
336 returns relative to both historical conditions and the high GHG emission scenarios. While SAI tends
337 to partially counteract the GHG-driven TWS changes in R1, R3, R4, and R5. Larger TWS levels are
338 expected for the entire MENA compared with the GHG climate alone, particularly in Iran, Iraq, and
339 the western NA. Nonetheless, compared to the historical period, the Arabian Peninsula (Fig. 5d) is
340 the region with the most robust increase in the extreme TWS under both the global warming and SAI
341 scenarios. Extreme TWS in its neighbor dry land of eastern NA with a hyper-arid climate is still
342 smaller than the historical conditions.

343

344 Table 2 quantitatively compares the differences between TWS (and its corresponding 95% lower and
345 upper bounds in Fig. 5) changes at 30-, 50-, and 100-yr return periods under historical, global
346 warming, and SAI scenarios. Global warming, on the whole, decreases the TWS extremes at 30- to
347 100-year return periods over all the study areas except for the Arabian Peninsula and western NA.
348 The most robust decreases in the extreme TWS imposed by global warming relative to historical
349 conditions occur in the lands around the Caspian (-42.5 Kg/m^2 on average over return periods from
350 30- to 100-year) and Mediterranean (-17.6 Kg/m^2 on average) and the eastern NA (-5.71 Kg/m^2 on
351 average) are partially suppressed by SAI. A small decrease in the extreme TWS in Iran and Iraq
352 simulated under GHG (-2.8 Kg/m^2) is overcompensated by SAI ($+21.0 \text{ Kg/m}^2$). Although SAI
353 decreases the TWS in the Arabian Peninsula (-2.2 Kg/m^2) relative to global warming, it still tends to
354 experience the most robust extreme water storage increases in the future compared with historical
355 conditions. In western NA, the SAI simulation slightly intensifies the increased extreme TWS imposed
356 by high GHG emissions by $+1.9 \text{ Kg/m}^2$. Although SAI partially compensates for the changes over most
357 of the study area (positive SSP5-8.5-SAI minus SSP5-8.5 values in Table 2), on the whole, extreme
358 TWS tend to increase in the dry regions of Iran and Iraq, the Arabian Peninsula, and western NA while
359 substantially decreasing in the wetter lands around the Caspian and Mediterranean Seas, and to
360 lower degrees, in the eastern NA as a more continental dry land compared with historical conditions.

361



362

363

364

365

366

367

368

Figure 5. The TWS anomaly return level versus return period using the first three realizations for the historical, SSP5-8.5, and SSP5-8.5-SAI in regions 1 to 6 (a to d). The two parallel dashed black lines refer to 30- (left) and 50-year (right) return periods. Shading in each curve is the 95% upper and lower confidence bands.



369 **Table 2.** The differences (in Kg/m²) between the medians of the TWS return level at 30-, 50-, and
 370 100-year return periods using the first three realizations for the historical, SSP5-8.5, and SSP5-8.5-
 371 SAI. Consistently, the value inside the parenthesis is the difference-range values between lowers
 372 and uppers 95% confidence intervals from different scenarios.

Region	SSP5-8.5 minus Historical			SSP5-8.5-SAI minus Historical			SSP5-8.5-SAI minus SSP5-8.5		
	30-yr	50-yr	100-yr	30-yr	50-yr	100-yr	30-yr	50-yr	100-yr
R1	-42.7 (-42.9, -42.6)	-42.5 (-42.6, -42.3)	-42.2 (-42.4, -42.1)	-22.4 (-22.9, -22.0)	-23.1 (-23.7, -22.4)	-23.6 (-24.4, -22.8)	20.3 (19.7, 20.9)	19.4 (18.7, 20.2)	18.7 (17.7, 19.6)
R2	-4.3 (-5.0, -3.6)	-3.0 (-3.8, -2.2)	-1.2 (-2.4, -0.1)	21.0 (20.9, 21.1)	21.1 (21.0, 21.2)	21.0 (20.9, 21.1)	25.3 (24.7, 25.9)	24.1 (23.3, 24.8)	22.2 (21.2, 23.3)
R3	-19.1 (-20.1, -18.0)	-17.8 (-19.3, -16.4)	-16.1 (-18.1, -14.1)	-12.5 (-12.8, -12.2)	-12.7 (-13.1, -12.2)	-12.8 (-13.4, -12.2)	6.6 (5.2, 7.9)	5.2 (3.3, 7.0)	3.3 (0.7, 5.9)
R4	23.6 (22.6, 24.6)	25.4 (24.0, 26.7)	28.0 (26.0, 30.0)	24.1 (23.9, 24.2)	23.9 (23.6, 24.2)	23.5 (23.0, 23.9)	0.5 (-0.6, 1.6)	-1.5 (-3.1, 0.2)	-4.6 (-7.0, -2.1)
R5	-5.78 (-5.79, -5.77)	-5.75 (-5.78, -5.72)	-5.60 (-5.65, -5.50)	-1.45 (-1.50, -1.40)	-1.45 (-1.50, -1.40)	-1.40 (-1.50, -1.30)	4.40 (4.30, 4.45)	4.30 (4.30, 4.35)	4.30 (4.10, 4.30)
R6	4.70 (4.68, 4.73)	4.75 (4.70, 4.80)	4.6 (4.5, 4.7)	5.8 (5.5, 6.1)	6.5 (6.1, 6.9)	7.5 (6.9, 8.1)	1.1 (0.8, 1.4)	1.8 (1.3, 2.2)	2.9 (2.2, 3.6)

373

374

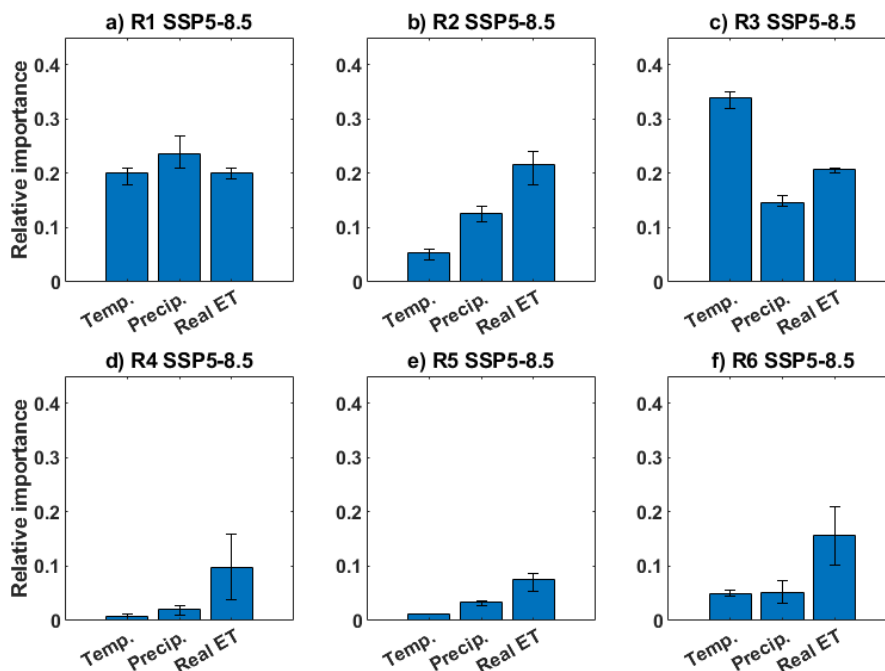
375 3.3 Drivers of TWS change

376 To assess which variables have the most impact on mean TWS under both global warming and SAI,
 377 we fitted an MLR model to each ensemble member separately in each of the six regions (Figs. 6 and
 378 7). The most important variable for the mean TWS is region-specific. In lands around the Caspian Sea
 379 (R1), precipitation is the most important variable for TWS while temperature is a primary driver in
 380 lands around the Mediterranean. The real ET is the most important variable in dry regions R2, R4 to
 381 R6 under both GHG forcing (Fig. 6) and the SAI except for one case (R5 under the SAI in Fig. 7).
 382 Warmer climate enhances the atmospheric water content over regions and seasons (Cook et al.,
 383 2020) since 1°C warming is accompanied by ~7% enhancement in the air water storage capacity
 384 (Trenberth, 2011), and, in turn, increases the evaporative demand (Arnell, 1999), and vice versa for
 385 cooler conditions. Real ET itself is mostly controlled by temperature and available water for
 386 evaporation (i.e., precipitation, soil moisture, and vegetation coverage). With just temperature and
 387 precipitation as independent variables, we find that the temperature under both global warming and
 388 SAI is generally more important for TWS than precipitation over the Mediterranean wet region due
 389 to evapotranspiration. In contrast, precipitation plays a stronger role on TWS in the lands around the
 390 Caspian Sea with lower precipitation as well as all dry regions (except for R5 under SAI) under both
 391 future climate scenarios.

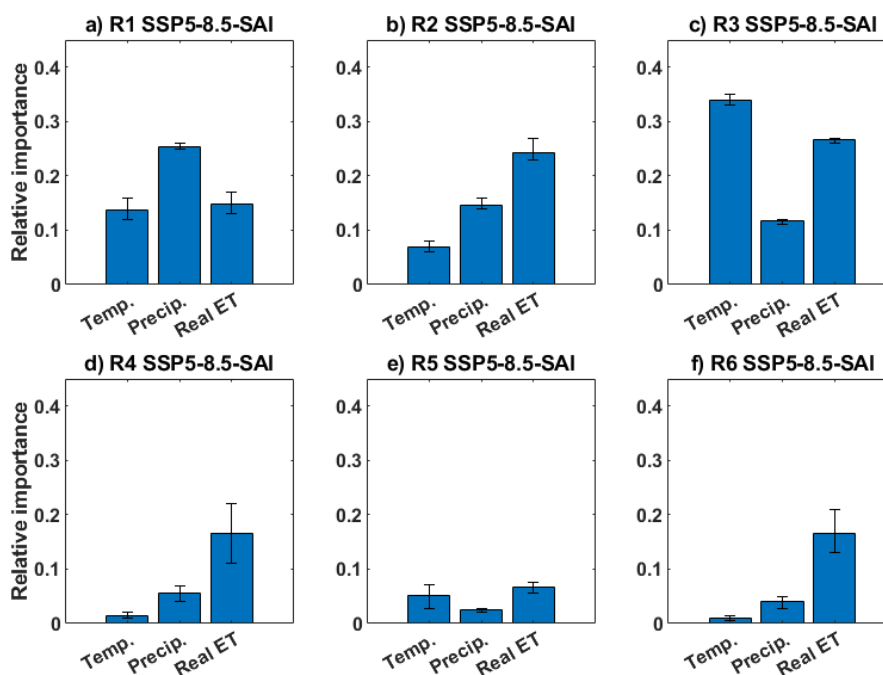
392



393 The regression models indicate that TWS is mostly driven by the combined impacts of changes in
 394 both temperature and precipitation, consistent with the fact that precipitation is not the only
 395 controlling factor for water resources (Cook et al., 2014; Wu et al., 2020). However, the temperature
 396 in the Mediterranean area with the highest precipitation over the entire domain studied plays a more
 397 important role than both real EV and precipitation under both warming and SAI scenarios.
 398 Caution is required when interpreting the relative importance results for the arid regions of R4 to R6
 399 as their variance explained ($R^2=0.3$ to 0.45) from the MLR models is smaller than those (up to 0.8)
 400 for the wetter lands around the Caspian and Mediterranean Seas. This, most probably, arises from
 401 the arid to hyper-arid climate of R4 to R6 with a small and irregular annual precipitation, and, in turn,
 402 irregular TWS anomaly time series (Figs. 2d, e, and f).
 403
 404



405
 406 **Figure 6.** LMG importance plot (Lindeman et al., 1980) of the three independent variables in the
 407 regression for TWS for the global warming SSP5-8.5 scenario in each region. The bar and range-bar
 408 respectively show the ensemble mean importance and the range of importance from the three
 409 ensemble members.



410

411

412

Figure 7. As in Fig. 6, but for the SSP5-8.5-SAI scenario.

413 **4. Discussion**

414 We have analyzed the potential impacts of the unmitigated global warming SSP5-8.5 scenario (GHG)
 415 and the same GHG emissions trajectory with the addition of SAI (GHG+SAI) on both the mean and
 416 extreme water storage across the lands around the Caspian and Mediterranean Seas, Middle East,
 417 and NA. We have used the CESM2(WACCM) climate model simulations with three realizations of each
 418 historic and SSP5-8.5-SAI scenario and five available realizations for SSP5-8.5. In response to high
 419 GHG emission over the 2071-2100 period, the mean TWS decreases in the wetter regions (i.e., around
 420 the Caspian and Mediterranean Seas) while, on the whole, it increases or shows no significant change
 421 in the dry areas of MENA. The mean TWS increase in the southern MENA is consistent with other
 422 climate model simulations showing increased precipitation and soil moisture in CMIP6 simulations
 423 under SSP5-8.5 (Cook et al., 2020), and SSP2-4.5 (Ajjur et al., 2021; Scanlon et al., 2023). The decrease
 424 in mean TWS in the Mediterranean projected under the global warming SSP5-8.5 with
 425 CESM2(WACCM) here is also in agreement with the previous studies based on SSP5-8.5 (e.g., Cook et
 426 al., 2020; Scanlon et al., 2023), RCP2.6 and RCP4.5 (e.g., Döll et al., 2018). It is also consistent with
 427 projections from 11 global hydrological models (Schewe et al., 2014) with globally forced 2°C
 428 warming (Schleussner et al., 2016).



429

430 The SSP5-8.5-SAI scenario tends to reverse, to a degree, the significant changes in mean TWS
431 imposed by SSP5-8.5 over the entire MENA. Although the decreased TWS in the wetter lands around
432 the Caspian and Mediterranean Seas driven by the GHG SSP5-8.5 scenario (Fig. 3b) was partially
433 reversed by the SAI (Fig. 3d) here, the mean TWS deficit is not fully canceled out by the intervention
434 (Figs., 3c, 4a, and 4c). However, SAI causes the dry MENA regions (Fig. 3d), particularly Iran, Iraq, and
435 the Arabian Peninsula, to have higher mean water storage relative to the historical period (Figs. 3c
436 and 4).

437

438 Since most parts of the Middle East already suffer from water shortage, SAI appears to improve the
439 water status across the area, particularly in the dry regions of Iran, Iraq, and the Arabian Peninsula
440 as compared with the pure GHG forced scenario. SAI may decrease the vulnerability of the region to
441 changing climate conditions. This is important in the context of substantial population growth during
442 the past half a century which is expected to continue albeit at a lower rate (Oroud, 2008).

443

444 We also compared the changes in TWS with changes in precipitation, temperature, real ET, soil
445 moisture, and potential ET over each region under both global warming and SAI scenarios (Figs. S2
446 to S6 in the Supplementary Information). The TWS decreasing patterns across the entire study area
447 are similar to soil moisture change patterns (Fig. S2 and S4 in Supplementary Information) but more
448 widespread than precipitation under global warming (Fig. S4). The decreased TWS is seen beyond
449 the regions of reduced precipitation (Fig. S4), from beyond the Mediterranean and Atlantic coasts to
450 include Syria, Iraq, and the lands around the Caspian Sea as well as to a wide portion of NA (Fig. 4).
451 These include places where precipitation is either increasing or shows no significant change,
452 consistent with results reported by Cook et al. (2020). The most robust decreases in TWS occur over
453 the Mediterranean (Fig. 4c) where the substantial precipitation decrease (region-wide averaged 76
454 mm yr⁻¹ or 15.8% in Fig. S5) is amplified by a significant increase in air temperature (4 °C based on
455 medians in Fig. S5) in response to the increased GHG emission compared with present-day
456 conditions. Similarly, a decrease in precipitation (Kim and Byun, 2009) and surface runoff (Cook et
457 al., 2020) has been reported across Mediterranean coasts under GHG warming.

458

459 The more robust and widespread deficit in mean TWS compared to precipitation in the area
460 highlights the profound roles that other variables/processes have on the increased ET such as greater
461 atmospheric moisture demand (Dai et al., 2013, 2018) and greater vegetation water use (Mankin et



462 al., 2019) owing to warmer conditions under global warming, consistent with regression model
463 results. Furthermore, although precipitation over a broad portion of MENA is lowered under SAI
464 relative to global warming, the mean TWS, in general, increases across a broad portion of the MENA
465 region in response to the intervention. TWS significantly increases over Iran and Iraq under SAI
466 compared to historical and global warming (Fig. 4b) as gains in available water from decreased
467 temperature and, in turn, EV is largely sufficient to compensate for decreased precipitation (Fig. S3
468 and S5), signifying that in addition to precipitation, the water storage also strongly depends on local
469 temperature (Ajjur et al., 2021). As an example, around the Caspian Sea (R1), although the changes
470 in precipitation imposed by global warming are simulated to have been fully restored by SAI, the
471 temperature has not; and in turn, the TWS is not fully restored by SAI. This is consistent with MLR
472 model results (Fig. 7a) in which, beyond the precipitation, temperature also plays an important role
473 in TWS across R1.

474

475 Our findings, on the whole, suggest that the specific SAI scenario considered here helps water storage
476 in the dry regions (R2, R4, R5, and R6), i.e., leads to higher soil moisture and TWS compared with
477 both the historical conditions and pure GHG-induced global warming. This works through the
478 combined positive effects of (1) a substantial decrease in temperature and ET over the entire study
479 area compared with SSP5-8.5 global warming, and (2) the increased precipitation in the southern
480 MENA dry regions relative to historical conditions. However, the wet and colder regions, particularly
481 around the Mediterranean coasts, may have less water storage compared with the historical period
482 but more water relative to the GHG scenario due to a significant decrease in evapotranspiration
483 under SAI.

484

485 Based on the return level-period analyses, the extreme ends of the TWS probability distribution
486 changes (Fig. 5 and Table 2) due to SAI are significant relative to both the historical period and global
487 warming, except in one case (in R3 compared to global warming (Fig. 5c)), particularly in the lands
488 around the Caspian and Mediterranean Seas and the Arabian Peninsula where the global warming-
489 imposed changes are large. SAI significantly reverses the decreased extreme TWS in the northern
490 lands of the domain as well as having enhanced extreme TWS across the Arabian Peninsula.
491 Moreover, in the dry regions of Iran and Iraq (R2) and western NA (R6), SAI significantly increases
492 the extreme TWS relative to both the historical conditions and global warming (Figs. 5b and 5f and
493 Table 2). In contrast, in the hyper-arid region of eastern NA, although SAI compensates for the
494 decreased extreme TWS, it is still smaller than the historical conditions.



495

496 The extreme TWS under the high GHG emission scenario significantly decreases over the land around
497 the Caspian (-42.5 Kg/m² on average over return periods from 30- to 100-year) and Mediterranean
498 (-17.6 Kg/m² on average) as well as eastern NA (-5.71 Kg/m² on average) but increases in the dry
499 regions of the Arabian Peninsula (+25.7 Kg/m²) and western NA (+4.7 Kg/m²). SAI partially
500 suppresses the changes imposed by global warming except for Iran and Iraq (R2) and the western
501 NA (R6) where it significantly increases the extreme TWS. The extreme TWS does not show
502 significant changes in Iran and Iraq under global warming, but SAI substantially increases the
503 extremes relative to global warming (+24.0 Kg/m²). Although SAI partially compensates for the
504 changes in most of the study area (positive SSP5-8.5-SAI minus SSP5-8.5 values in Table 2), on the
505 whole, the extreme TWS tends to increase in dry regions of Iran and Iraq, Arabian Peninsula, and
506 western NA while substantially decrease in the wetter lands around the Caspian and Mediterranean
507 Seas, and to lower degrees, in the eastern NA compared to historical conditions.

508

509 Both future climate scenarios (SSP5-8.5 and SSP5-8.5-SAI) indicate significant changes to TWS
510 relative to historical around the Caspian and Mediterranean Seas, Middle East, and NA which will
511 have important hydrological consequences in terms of the drought and flood disasters. Some dry
512 areas such as Iran, Iraq, and the Arabian Peninsula are projected to receive greater extreme TWS
513 under both global warming and SAI or only SAI, and these regions have suffered historically from
514 flooding (e.g., Abbaspour et al., 2009; Ghavidel and Jafari Hombari, 2020; Dezfuli et al., 2021). The
515 significant increase in extreme TWS enhances their flood risks. Hence, governments in these regions
516 should plan for adaptations to water megastructures such as the dams on the large rivers of Karkheh
517 and Karun in western Iran and the Euphrates and Tigris in Iraq, since they have been mostly designed
518 with historical hydrology in mind.

519

520 There are several caveats and caution needed for our results. First, our findings are based on a single
521 model simulation (CESM2) and a single scenario climate scenario SSP5-8.5 with (three available
522 realizations) and without (five available realizations). Future studies should consider alternative SAI
523 scenarios to explore the sensitivity of our results to model and scenario choices. The SSP scenarios
524 include some that clearly portray undesirable futures, especially the high emissions SSP5 scenarios
525 or the regional rivalry SSP3 that illustrate the danger of unchecked climate change (MacMartin et al.,
526 2022). There are more caveats for the SAI experiment used here (1) it deploys in 2020, therefore
527 does not simulate any plausible future, and (2) takes into account solely the high-emissions scenario



528 SSP5-8.5 that is suitable for capturing a high “signal” compared to internal variability. This is useful
529 for understanding the science but inconsistent with present-day projections of mitigation attempts
530 (Burgess et al., 2020). However, while the signal is stronger under high GHG emissions, it is plausible
531 that the directions and patterns of response would be similar in a lower-emission experiment, with
532 the magnitude of changes roughly depending on the degree of warming being suppressed by SAI (e.g.,
533 MacMartin et al., 2019).

534

535 5. Conclusions

536 The current study is the first attempt for understanding the influence of GHG emission and SAI
537 scenarios on both mean and extreme water storage changes over the lands around the Caspian and
538 Mediterranean Seas, Middle East, and northern Africa under global warming and SAI scenarios
539 compared to the historical 1985-2014 conditions. The mean TWS is projected to decrease across the
540 wetter lands around the Caspian and Mediterranean Seas to the north (35-58 Kg/m² on average) but
541 increase over the most MENA region (up to 75.5 Kg/m² over the Arabian Peninsula) that has a drier
542 climate under the high GHG forcing compared to the present-day conditions.

543

544 Although the SAI tends to reverse, to a degree, the significant changes in TWS revealed by SSP5-8.5
545 over the entire area, it significantly overcompensates for the slightly reduced TWS under the high
546 GHG scenario in Iran and Iraq. MLR model analysis of driving factors suggests that the impacts of
547 temperature on water storage changes, like precipitation, are also important under both high GHG
548 forcing and SAI scenarios. Although SAI mostly decreases precipitation over most of the domain, it is
549 accompanied by higher mean TWS across the entire study area due to the cooler climate.

550

551 Although significant changes in the extreme TWS under high GHG emissions are reduced by SAI, the
552 changes due to both future climate changes are still large relative to the historical period across a
553 broad portion of the domain. With SAI, TWS significantly decreases in the eastern lands around the
554 Caspian Sea while substantially increasing across the Middle East regions of Iran, Iraq, and the
555 Arabian Peninsula. This may increase flood risks since water megastructures have been mostly
556 designed with historical hydrology in mind. Finally, the SAI scenario appears to increase accessible
557 water storage in the dry regions of the Middle East and northern Africa. The wetter and colder lands
558 around the Caspian and Mediterranean Seas may have less available water compared with the
559 historical conditions, although SAI partially ameliorates the changes imposed by global warming.

560



561

562 **Data availability:**

563 The data for CESM2 simulations are publicly available via its website: [https://esgf-](https://esgf-node.llnl.gov/search/cmip6/)
564 [node.llnl.gov/search/cmip6/](https://esgf-node.llnl.gov/search/cmip6/).

565

566 **Acknowledgments:**

567 This research has been supported by the DEGREES Initiative in collaboration with the World
568 Academy of Sciences (grant no. 4500443035).

569

570 **Conflict of Interest:**

571 There is no conflict of interest.

572

573 **References:**

574 Abbaspour, K. C., Faramarzi, M., Ghasemi, S. S., & Yang, H. (2009). Assessing the impact of climate
575 change on water resources in Iran. *Water resources research*, 45(10).

576 Abiodun, B. J., Odoulami, R. C., Sawadogo, W., Oloniyo, O. A., Abatan, A. A., New, M., ... & MacMartin, D.
577 G. (2021). Potential impacts of stratospheric aerosol injection on drought risk managements
578 over major river basins in Africa. *Climatic Change*, 169(3), 1-19.

579 Ajjur, S. B., & Al-Ghamdi, S. G. (2021). Evapotranspiration and water availability response to climate
580 change in the Middle East and North Africa. *Climatic Change*, 166(3-4), 28.

581 Arnell, N. W. (1999). Climate change and global water resources. *Global environmental change*, 9,
582 S31-S49.

583 Azzopardi, B., Balzan, M. V., Cherif, S., Doblaz-Miranda, E., dos Santos, M., Dobrinski, P., ... & Xoplaki, E.
584 (2020). Climate and environmental change in the Mediterranean basin–current situation and
585 risks for the future. *First Mediterranean assessment report*.

586 Bala, G., Duffy, P. B., & Taylor, K. E. (2008). Impact of geoengineering schemes on the global
587 hydrological cycle. *Proceedings of the National Academy of Sciences*, 105(22), 7664-7669.

588 Barlow, M., Zaitchik, B., Paz, S., Black, E., Evans, J., & Hoell, A. (2016). A review of drought in the Middle
589 East and southwest Asia. *Journal of climate*, 29(23), 8547-8574.

590 Bland, J. M., & Altman, D. G. (1995). Multiple significance tests: the Bonferroni
591 method. *Bmj*, 310(6973), 170.

592 Breiman, L. (1996). Bagging predictors. *Machine learning*, 24, 123-140.



- 593 Bucchignani, E., Mercogliano, P., Panitz, H.-J., & Montesarchio, M. (2018). Climate change projections
594 for the Middle East–North Africa domain with COSMO-CLM at different spatial resolutions.
595 *Advances in Climate Change Research*, 9(1), 66–80. <https://doi.org/10.1016/j.>
596 *Accre.2018.01.004*
- 597 Burgess, M. G., Ritchie, J., Shapland, J., & Pielke, R. (2020). IPCC baseline scenarios have over-projected
598 CO₂ emissions and economic growth. *Environmental Research Letters*, 16(1), 014016.
- 599 Byun, H. R., & Wilhite, D. A. (1999). Objective quantification of drought severity and duration. *Journal*
600 *of climate*, 12(9), 2747-2756.
- 601 Cook, B. I., Mankin, J. S., Marvel, K., Williams, A. P., Smerdon, J. E., & Anchukaitis, K. J. (2020). Twenty-
602 first century drought projections in the CMIP6 forcing scenarios. *Earth's Future*. 8,
603 e2019EF001461.
- 604 Cook, B. I., Anchukaitis, K. J., Touchan, R., Meko, D. M., & Cook, E. R. (2016). Spatiotemporal drought
605 variability in the Mediterranean over the last 900 years. *Journal of Geophysical Research:*
606 *Atmospheres*, 121(5), 2060-2074.
- 607 Cook, B. I., Smerdon, J. E., Seager, R., & Coats, S. (2014). Global warming and 21 st century
608 drying. *Climate dynamics*, 43, 2607-2627.
- 609 Crook, J. A., Jackson, L. S., Osprey, S. M., & Forster, P. M. (2015). A comparison of temperature and
610 precipitation responses to different Earth radiation management geoengineering
611 schemes. *Journal of Geophysical Research: Atmospheres*, 120(18), 9352-9373.
- 612 Cheng, W., MacMartin, D. G., Dagon, K., Kravitz, B., Tilmes, S., Richter, J. H., ... & Simpson, I. R. (2019).
613 Soil moisture and other hydrological changes in a stratospheric aerosol geoengineering large
614 ensemble. *Journal of Geophysical Research: Atmospheres*, 124(23), 12773-12793.
- 615 Dai, A. (2013). Increasing drought under global warming in observations and models. *Nature climate*
616 *change*, 3(1), 52-58.
- 617 Dezfuli, A., Bosilovich, M. G., & Barahona, D. (2021). A dusty atmospheric river brings floods to the
618 Middle East. *Geophysical Research Letters*, 48(23), e2021GL095441.
- 619 Dagon, K., & Schrag, D. P. (2016). Exploring the effects of solar radiation management on water
620 cycling in a coupled land–atmosphere model. *Journal of Climate*, 29(7), 2635-2650.
- 621 Doksum, K. A., & Sievers, G. L. (1976). Plotting with confidence: Graphical comparisons of two
622 populations. *Biometrika*, 63(3), 421-434.
- 623 Döll, P., Trautmann, T., Gerten, D., Schmied, H. M., Ostberg, S., Saaed, F., & Schleussner, C. F. (2018).
624 Risks for the global freshwater system at 1.5 C and 2 C global warming. *Environmental*
625 *Research Letters*, 13(4), 044038.



- 626 Döll, P.; Flörke, M. Global-Scale Estimation of Diffuse Groundwater Recharge; Institute of Physical
627 Geography, Frankfurt University: Frankfurt am Main, Germany, 2005; Available online:
628 https://www.uni-frankfurt.de/45217767/FHP_03_Doell_Floerke_2005.pdf.
- 629 Droogers, P., Immerzeel, W. W., Terink, W., Hoogeveen, J., Bierkens, M. F. P., Van Beek, L. P. H., &
630 Debele, B. (2012). Water resources trends in Middle East and North Africa towards
631 2050. *Hydrology and Earth System Sciences*, 16(9), 3101-3114.
- 632 Evans, J. P., & Smith, R. B. (2006). Water vapor transport and the production of precipitation in the
633 eastern Fertile Crescent. *Journal of Hydrometeorology*, 7(6), 1295-1307.
- 634 Eyring, V., Bony, S., Meehl, G. A., Senior, C. A., Stevens, B., Stouffer, R. J., & Taylor, K. E. (2016). Overview
635 of the Coupled Model Intercomparison Project Phase 6 (CMIP6) experimental design and
636 organization. *Geoscientific Model Development*, 9(5), 1937-1958.
- 637 Fader M., Shi S., Von Bloh W., Bondeau A., Cramer W. (2016). Mediterranean irrigation under climate
638 change: More efficient irrigation needed to compensate for increases in irrigation water
639 requirements. *Hydrol. Earth Syst. Sci.* 20, 953-973. doi: 10.5194/hess-20-953-2016
- 640 Famiglietti, J. S. (2014). The global groundwater crisis. *Nature Climate Change*, 4(11), 945-948.
- 641 Faour, G., Mhaweij, M., & Fayad, A. (2016). Detecting changes in vegetation trends in the Middle East
642 and North Africa (MENA) region using SPOT vegetation. *Cybergeog: European Journal of*
643 *Geography*.
- 644 Fragaszy, S. R., Jedd, T., Wall, N., Knutson, C., Fraj, M. B., Bergaoui, K., ... & McDonnell, R. (2020).
645 Drought Monitoring and Warning System for the Middle East and North Africa. *Bulletin of the*
646 *American Meteorological Society*, 101(10), 904-910.
- 647 Ghavidel, Y., & Jafari Hombari, F. (2020). Synoptic analysis of unexampled super-heavy rainfall on
648 April 1, 2019, in west of Iran. *Natural hazards*, 104(2), 1567-1580.
- 649 Gilleland, E. (2020). Bootstrap methods for statistical inference. Part II: Extreme-value
650 analysis. *Journal of Atmospheric and Oceanic Technology*, 37(11), 2135-2144.
- 651 Giorgi, F., & Lionello, P. (2008). Climate change projections for the Mediterranean region. *Global and*
652 *Planetary Change*, 63(2-3), 90-104. <https://doi.org/10.1016/j.gloplacha.2007.09.005>
- 653 Giorgi F. (2006) Climate change hot-spots. *Geophys Res Lett* 33: L08707.
654 doi:10.1029/2006GL025734.
- 655 Govindasamy B., Caldeira K. (2000) Geoengineering Earth's radiation balance to mitigate CO2-
656 induced climate change. *Geophys Res Lett* 27:2141-2144.
- 657 Grömping, U. (2007). Relative importance for linear regression in R: the package relaimpo. *Journal of*
658 *statistical software*, 17, 1-27.



- 659 Hofste, R. W., Reig, P., & Schleifer, L. (2019). 17 countries, home to one-quarter of the world's
660 population, face extremely high water stress.
- 661 Intergovernmental Panel on Climate Change (IPCC): Working Group I Contribution to the Sixth
662 Assessment Report (AR6), Climate Change 2021: The Physical Science Basis,
663 2021, <https://www.ipcc.ch/assessment-report/ar6/> (last access: 5 December 2022), 2021.
- 664 Johnson, J. W., & LeBreton, J. M. (2004). History and use of relative importance indices in
665 organizational research. *Organizational research methods*, 7(3), 238-257.
- 666 Karami, K., Tilmes, S., Muri, H., & Mousavi, S. V. (2020). Storm track changes in the Middle East and
667 North Africa under stratospheric aerosol geoengineering. *Geophysical Research*
668 *Letters*, 47(14), e2020GL086954.
- 669 Kim, D. W., & Byun, H. R. (2009). Future pattern of Asian drought under global warming
670 scenario. *Theoretical and Applied Climatology*, 98(1), 137-150.
- 671 Konapala, G., Mishra, A. K., Wada, Y., & Mann, M. E. (2020). Climate change will affect global water
672 availability through compounding changes in seasonal precipitation and evaporation. *Nature*
673 *communications*, 11(1), 3044.
- 674 Kravitz, B., et al. (2013), An energetic perspective on hydrological cycle changes in the
675 Geoengineering Model Intercomparison Project (GeoMIP), *J. Geophys. Res. Atmos.*, 118,
676 13,087–13,102, doi:10.1002/2013JD020502
- 677 Lelieveld, J., Hadjinicolaou, P., Kostopoulou, E., Chenoweth, J., El Maayar, M., Giannakopoulos, C., ... &
678 Xoplaki, E. (2012). Climate change and impacts in the Eastern Mediterranean and the Middle
679 East. *Climatic change*, 114, 667-687.
- 680 Lian, X., Piao, S., Chen, A., Huntingford, C., Fu, B., Li, L. Z., ... & Roderick, M. L. (2021). Multifaceted
681 characteristics of dryland aridity changes in a warming world. *Nature Reviews Earth &*
682 *Environment*, 2(4), 232-250.
- 683 Lindeman, R. H., Merenda, P. F., Gold, R. Z., (1980). Introduction to bivariate and multivariate
684 analysis (No. 04; QA278, L553.). Uniq ID: 5310754 Scott, Foresman, Glenview, IL.
- 685 Lionello, P., Malanotte-Rizzoli, P., Boscolo, R., Alpert, P., Artale, V., Li, L., ... & Xoplaki, E. (2006). The
686 Mediterranean climate: an overview of the main characteristics and issues. *Developments in*
687 *earth and environmental sciences*, 4, 1-26.
- 688 MacMartin, D. G., Vioni, D., Kravitz, B., Richter, J. H., Felgenhauer, T., Lee, W. R., ... & Sugiyama, M.
689 (2022). Scenarios for modeling solar radiation modification. *Proceedings of the National*
690 *Academy of Sciences*, 119(33), e2202230119.



- 691 Masson-Delmotte, V., Zhai, P., Pörtner, H. O., Roberts, D., Skea, J., & Shukla, P. R. (2022). Global
692 Warming of 1.5° C: IPCC Special Report on Impacts of Global Warming of 1.5° C above Pre-
693 industrial Levels in Context of Strengthening Response to Climate Change, Sustainable
694 Development, and Efforts to Eradicate Poverty. Cambridge University Press.
- 695 Milly, P. C., Dunne, K. A., & Vecchia, A. V. (2005). Global pattern of trends in streamflow and water
696 availability in a changing climate. *Nature*, 438(7066), 347-350.
- 697 Mooney, H., Cropper, A. & Reid, W. Confronting the human dilemma. *Nature* 434, 561--562 (2005).
- 698 Muthyala, R., Bala, G., & Nalam, A. (2018). Regional scale analysis of climate extremes in an SRM
699 geoengineering simulation, Part 1: precipitation extremes. *Current Science*, 1024-1035.
- 700 Oroud, I. M. (2008). The impacts of climate change on water resources in Jordan. *Climatic changes*
701 and water resources in the Middle East and North Africa, 109-123.
- 702 Peel, M. C., Finlayson, B. L., & McMahon, T. A. (2007). Updated world map of the Köppen-Geiger
703 climate classification. *Hydrology and earth system sciences*, 11(5), 1633-1644.
- 704 Ricke, K. L., Morgan, M. G., & Allen, M. R. (2010). Regional climate response to solar-radiation
705 management. *Nature Geoscience*, 3(8), 537-541.
- 706 Reiter, L., Falk, H., Groat, C. & Coussens, C. M. (eds) *From Source Water to Drinking Water: Workshop*
707 *Summary* (National Academies Press, Washington DC, 2004).
- 708 Robock, A., Oman, L., & Stenchikov, G. L. (2008). Regional climate responses to geoengineering with
709 tropical and Arctic SO₂ injections. *Journal of Geophysical Research: Atmospheres*, 113(D16).
- 710 Schewe, J., Heinke, J., Gerten, D., Haddeland, I., Arnell, N. W., Clark, D. B., Dankers, R., Eisner, S., Fekete,
711 B. M., ColonGonzalez, F. J., Gosling, S. N., Kim, H., Liu, X., Masaki, Y., Portmann, F. T., Satoh, Y.,
712 Stacke, T., Tang, Q., Wada, Y., Wisser, D., Albrecht, T., Frieler, K., Piontek, F., Warszawski,
713 L., and Kabat, P.: Multimodel assessment of water scarcity under climate change, *P. Natl. Acad.*
714 *Sci.*, 111, 3245–3250, doi:10.1073/pnas.1222460110, 2014
- 715 Shaban, A. (2008). Impact of climate change on water resources of Lebanon: Indications of
716 hydrological droughts. *Climatic changes and water resources in the Middle East and North*
717 *Africa*, 125-143.
- 718 Shiklomanov, I. A. & Rodda, J. C. (eds) *World Water Resources at the Beginning of the 21st Century*
719 (Cambridge Univ. Press, Cambridge, 2003).
- 720 Simpson, I. R., Tilmes, S., Richter, J. H., Kravitz, B., MacMartin, D. G., Mills, M. J., ... & Pendergrass, A. G.
721 (2019). The regional hydroclimate response to stratospheric sulfate geoengineering and the
722 role of stratospheric heating. *Journal of Geophysical Research: Atmospheres*, 124(23),
723 12587-12616.



- 724 Scanlon, B. R., Fakhreddine, S., Rateb, A., de Graaf, I., Famiglietti, J., Gleeson, T., ... & Zheng, C. (2023).
725 Global water resources and the role of groundwater in a resilient water future. *Nature*
726 *Reviews Earth & Environment*, 1-15.
- 727 Schleussner, C. F., Lissner, T. K., Fischer, E. M., Wohland, J., Perrette, M., Golly, A., ... & Schaeffer, M.
728 (2016). Differential climate impacts for policy-relevant limits to global warming: the case of
729 1.5 C and 2 C. *Earth system dynamics*, 7(2), 327-351.
- 730 Suppan, P., Kunstmann, H., Heckel, A., & Rimmer, A. (2008). Impact of climate change on water
731 availability in the Near East. *Climate changes and water resources in the Middle East and*
732 *North Africa*. Springer, Environmental Science and Engineering, Berlin.
- 733 Tabari, H., & Willems, P. (2018). Seasonally varying footprint of climate change on precipitation in
734 the Middle East. *Scientific reports*, 8(1), 4435.
- 735 Tilmes, S., MacMartin, D. G., Lenaerts, J., Van Kampenhout, L., Muntjewerf, L., Xia, L., ... & Robock, A.
736 (2020). Reaching 1.5 and 2.0 C global surface temperature targets using stratospheric aerosol
737 geoengineering. *Earth System Dynamics*, 11(3), 579-601.
- 738 Tilmes, S., Richter, J.H., Mills, M.J., Kravitz, B., MacMartin, D.G., Garcia, R.R., Kinnison, D.E., Lamarque,
739 J.F., Tribbia, J. and Vitt, F. (2018). Effects of different stratospheric SO₂ injection altitudes on
740 stratospheric chemistry and dynamics. *Journal of Geophysical Research:*
741 *Atmospheres*, 123(9), pp.4654-4673.
- 742 Tilmes, S., Fasullo, J., Lamarque, J. F., Marsh, D. R., Mills, M., Alterskjær, K., ... & Watanabe, S. (2013).
743 The hydrological impact of geoengineering in the Geoengineering Model Intercomparison
744 Project (GeoMIP). *Journal of Geophysical Research: Atmospheres*, 118(19), 11-036.
- 745 Trenberth, K. E. (2011). Changes in precipitation with climate change. *Climate research*, 47(1-2),
746 123-138.
- 747 Visioni, D., MacMartin, D. G., Kravitz, B., Boucher, O., Jones, A., Lurton, T., Martine, M., Mills, M. J., Nabat,
748 P., Niemeier, U., Séférian, R., and Tilmes, S.: Identifying the sources of uncertainty in climate
749 model simulations of solar radiation modification with the G6sulfur and G6solar
750 Geoengineering Model Intercomparison Project (GeoMIP) simulations, *Atmos. Chem. Phys.*,
751 21, 10039–10063, <https://doi.org/10.5194/acp-21-10039-2021>, 2021.
- 752 Wang, J., Song, C., Reager, J. T., Yao, F., Famiglietti, J. S., Sheng, Y., ... & Wada, Y. (2018). Recent global
753 decline in endorheic basin water storages. *Nature geoscience*, 11(12), 926-932.
- 754 Wilhite, D. A., & Buchanan-Smith, M. (2005). Drought as hazard: understanding the natural and social
755 context. *Drought and water crises: Science, technology, and management issues*, 3, 29.



- 756 World Bank (2017). Beyond Scarcity: Water Security in the Middle East and North Africa. The World
757 Bank.
- 758 Wu, W. Y., Lo, M. H., Wada, Y., Famiglietti, J. S., Reager, J. T., Yeh, P. J. F., ... & Yang, Z. L. (2020). Divergent
759 effects of climate change on future groundwater availability in key mid-latitude
760 aquifers. *Nature communications*, 11(1), 3710.
- 761 United Nations Educational Scientific and Cultural Organization. Water for People—Water for Life,
762 The United Nations World Water Development Report (Berghahn Books, Oxford, 2003)
- 763 Zittis, G., Hadjinicolaou, P., Klangidou, M., Proestos, Y., & Lelieveld, J. (2019). A multi-model, multi-
764 scenario, and multi-domain analysis of regional climate projections for the
765 Mediterranean. *Regional Environmental Change*, 19(8), 2621-2635.
- 766 Zhang, X., Li, J., Wang, Z., & Dong, Q. (2022). Global hydroclimatic drivers of terrestrial water storage
767 changes in different climates. *CATENA*, 219, 106598.